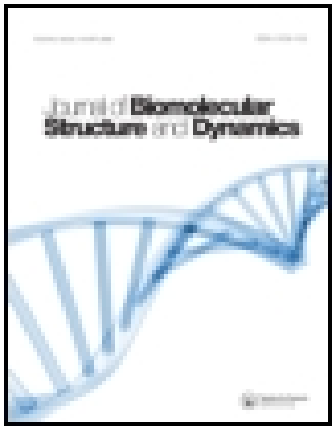

Journal of Biomolecular Structure and Dynamics
Publication details, including instructions for authors and subscription information:
http://www.tandfonline.com/loi/tbsd20

Role of inter-domain cavity in the attachment of the orange carotenoid protein to the phycobilisome core and to the fluorescence recovery protein

Dmitry V. Zlenko[a], Pavel M. Krasilnikov[a] & Igor N. Stadnichuk[b]
[a] Faculty of Biology, Lomonosov State University, 119234, Lenin Hills 1/12, Moscow, Russia
[b] A.N. Bakh Institute of Biochemistry RAS, 119071, Leninsky Prospekt 33/2, Moscow, Russia
Accepted author version posted online: 23 Apr 2015.Published online: 09 Jul 2015.

To cite this article: Dmitry V. Zlenko, Pavel M. Krasilnikov & Igor N. Stadnichuk (2015): Role of inter-domain cavity in the attachment of the orange carotenoid protein to the phycobilisome core and to the fluorescence recovery protein, Journal of Biomolecular Structure and Dynamics, DOI: 10.1080/07391102.2015.1042913

To link to this article: http://dx.doi.org/10.1080/07391102.2015.1042913

Journal of Biomolecular Structure and Dynamics, 2015
http://dx.doi.org/10.1080/07391102.2015.1042913

Role of inter-domain cavity in the attachment of the orange carotenoid protein to the phycobilisome core and to the fluorescence recovery protein

Dmitry V. Zlenko[a]*, Pavel M. Krasilnikov[a] and Igor N. Stadnichuk[b,1]

[a]*Faculty of Biology, Lomonosov State University, 119234, Lenin Hills 1/12, Moscow, Russia;* [b]*A.N. Bakh Institute of Biochemistry RAS, 119071, Leninsky Prospekt 33/2, Moscow, Russia*

Communicated by Ramaswamy H. Sarma

(*Received 18 November 2014; accepted 15 April 2015*)

Using molecular modeling and known spatial structure of proteins, we have derived a universal 3D model of the orange carotenoid protein (OCP) and phycobilisome (PBS) interaction in the process of non-photochemical PBS quenching. The characteristic tip of the phycobilin domain of the core-membrane linker polypeptide (L_{CM}) forms the attachment site on the PBS core surface for interaction with the central inter-domain cavity of the OCP molecule. This spatial arrangement has to be the most advantageous one because the L_{CM}, as the major terminal PBS-fluorescence emitter, accumulates energy from the most other phycobiliproteins within the PBS before quenching by OCP. In agreement with the constructed model, in cyanobacteria, the small fluorescence recovery protein is wedged in the OCP's central cavity, weakening the PBS and OCP interaction. The presence of another one protein, the red carotenoid protein, in some cyanobacterial species, which also can interact with the PBS, also corresponds to this model.

Keywords: allophycocyanin; fluorescence recovery protein; L_{CM}–polypeptide; orange carotenoid protein; phycobilisome (s); red carotenoid protein

1. Introduction

The primary light-harvesting antennae in cyanobacteria are phycobilisomes (PBS), giant phycobiliprotein complexes containing phycobilin chromophores. Cyanobacterial PBS consist of (i) a central tri-cylindrical core composed of disk-shaped allophycocyanin (APC) trimers and (ii) six lateral rods emanating fanlike from the core and built up of stacked hexamers of other phycobiliproteins (Adir, 2005; Watanabe & Ikeuchi, 2013). The short-term light adaptation process that reversibly increases thermal dissipation of excess energy in PBS (Rakhimberdieva, Stadnichuk, Elanskaya, & Karapetyan, 2004; Wilson et al., 2006) upon exposure of cyanobacteria to intense light, is called non-photochemical fluorescence quenching (NPQ). The water-soluble orange carotenoid protein (OCP) containing a single molecule of the keto-carotenoid 3′-hydroxyechinenone (Holt & Krogmann, 1981) is known to realize the NPQ of PBS (Kirilovsky & Kerfeld, 2013). The OCP exists in two forms: an inactive, dark-stable orange form (OCP^o) and a photoactive, metastable red form (OCP^r) that can be generated by intense blue-green light illumination (Wilson et al., 2008) and causes photoprotection through direct interaction with the PBS (Gwizdala, Wilson, & Kirilovsky, 2011; Stadnichuk et al., 2011).

The spatial localization of the OCP^r molecule in complex with the PBS is extremely important for evaluation of the molecular quenching mechanism. The large – two orders of magnitude (35 kDa vs. ~3–5 MDa) – difference between the molecular masses of OCP and PBS, respectively (Adir, 2005; Kerfeld, 2004), means that the attachment site of the OCP to the PBS has to be very specific. As the mutants lacking lateral PBS cylinders in the cyanobacterium *Synechocystis* sp. PCC 6803 (hereafter referred to as *Synechocystis*) were still capable of NPQ, the OCP^r binding site was attributed to the PBS core (Scott et al., 2006; Stadnichuk, Lukashev, & Elanskaya, 2009; Wilson et al., 2008). The tri-cylindrical core subcomplex (M ~ 1.2 MDa) consists of one upper and two basal cylinders; each of these is composed of four stacked $(\alpha\beta)_3$-APC trimer discs (Adir, 2005; Watanabe & Ikeuchi, 2013). X-ray diffraction studies on APC crystals have revealed that each $(\alpha\beta)_3$ disk is ~3 nm thick and has a diameter of ~11 nm which involves a central hole in diameter of ~3.5 nm (McGregor, Klartag, David, & Adir, 2008). The boomerang-shaped monomeric (αβ) units form a threefold symmetry of the $(\alpha\beta)_3$ trimer. The chromophores covalently bound to cysteine residues α81 and β81 are packed rigidly in their respective pigment-binding pockets. The PBS core also possesses three minor

*Corresponding author. Email: zoidberg@erg.biophys.msu.ru

[1]Current address: K.A.Timiryazev Institute of Plant Physiology RAS, 127726, Botanicheskaya 35, Moscow, Russia.

solely chromophorylated red-shifted polypeptides that replace corresponding α- and β-subunits of APC: ApcD (α^B), ApcF (β^{18}), and L_{CM} (ApcE, or anchor protein) (Adir, 2005; Watanabe & Ikeuchi, 2013). These polypeptides form in two basal cylinders four kinds of APC trimers: $(\alpha\beta)_3$, $(\alpha\beta)_3L_{7.8}$, $(\alpha\beta)_2(\alpha^B\beta)$, and $(\alpha\beta)_2(PBL_{CM}\beta^{18})$, where PBL_{CM} indicates the chromophorylated domain of 90 kDa L_{CM} polypeptide and $L_{7.8}$ – a small colorless linker polypeptide (Figure 1). Unlike ApcD and ApcF (Jallet, Gwizdala, & Kirilovsky, 2012; Stadnichuk et al., 2012), the interaction of OCP with purified L_{CM} *in vitro* completed with the use of some spectral and biochemical methods *in vivo* indicated that OCP quenches the PBL_{CM}-chromophore (Stadnichuk et al., 2012, 2013).

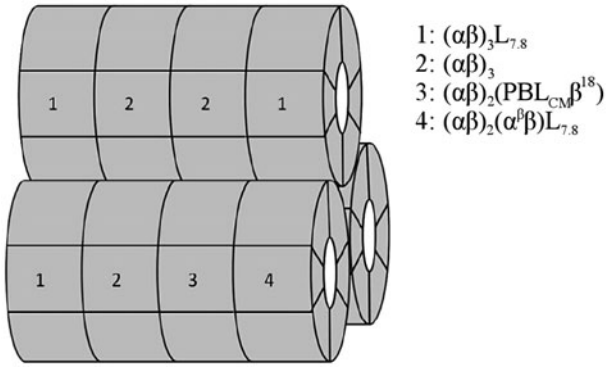

Figure 1. Schematic representation of the tricylindrical PBS core of *Synechocystis*. Each cylinder consists of four discs and each disc represents a trimer composed of six phycobiliprotein subunits – each of them contains one phycobilin chromophore. Numbering refers the corresponding subunit composition of the disc. While the top cylinder contains only APC trimers – with or without the small $L_{7.8}$-linker – the two compositionally identical bottom cylinders, adjacent to the thylakoid membrane, also contain three terminal emitters, ApcD, ApcF, and PB domain of L_{CM} (ApcE) as indicated. Reproduced from (Stadnichuk et al., 2013).

As the crystallographic and NMR data for the PBS, OCP^r, and L_{CM} are unavailable, the most probable mutual spatial arrangement of the OCP and PBS in their complex was modeled *in silico* (Stadnichuk et al., 2013) by a docking procedure using the crystal structures of OCP^o (Kerfeld, 2004) and APC (Brejc, Ficner, Huber, & Steinbacher, 1995). The OCP is composed of N- and C-terminal domains separated by a big central cavity; the carotenoid spans both domains (Kerfeld, 2004; Wilson et al., 2010). The total cavity-volume equal to 895 $Å^3$ was proposed by Kerfeld (2004) large enough for a substantial interaction with another protein. It turned out that the characteristic tip on the lateral surface of the APC trimer and the intra-domain cavity of the OCP molecule form the model of the probable site of the OCP and PBS interaction (Figure 2 and Stadnichuk et al., 2013). In the present work, we demonstrate that the PBL_{CM}-domain, being highly homologous to the αAPC (Gao et al., 2012; McGregor et al., 2008), could substitute for it in APC trimer using molecular modeling methods. The developed 3D model of the OCP–$(\alpha\beta)_2(PBL_{CM}\beta^{18})$ supercomplex fully corresponds to the interaction of the OCP and PBS through the established biochemical instrumentality of OCP and L_{CM} (Stadnichuk et al., 2012, 2013).

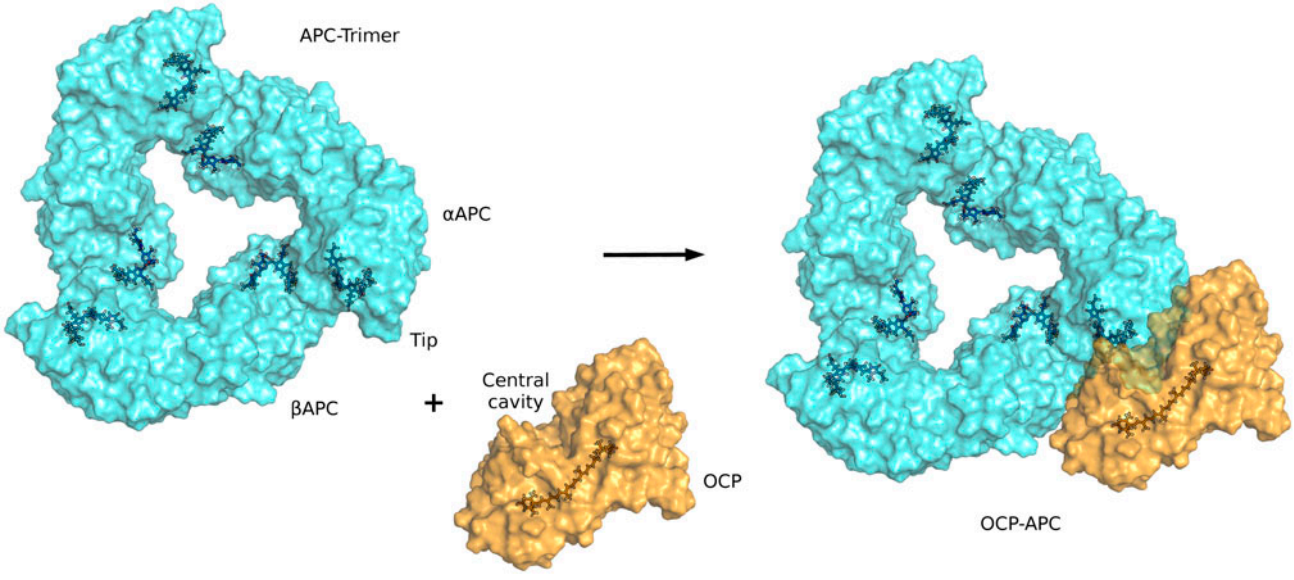

Figure 2. Molecular model of OCP-APC complex. Constructed 3D model showing the attachment of OCP (orange) to the APC trimer (cyan); carotenoid (dark orange) and phycobilin (dark blue) chromophores here and in Figure 6 and 8 are shown as dark sticks. Reproduced from (Stadnichuk et al., 2013) with alterations.

The fluorescence recovery protein (FRP) whose crystal structure was recently established (Sutter et al., 2013), is a 13 kDa protein that does not bind a chromophore and is found in cyanobacterial species that also contain the OCP (Boulay, Wilson, D'Haene, & Kirilovsky, 2010; Sutter et al., 2013). FRP is known to accelerate the reversibility of the NPQ process in the dark (Boulay et al., 2010) and, like PBS, interacts with the red active form of OCP (Gwizdala, Wilson, Omari-Nasser, & Kirilovsky, 2013). By a docking procedure, in agreement with the particular role of the OCP intra-domain cavity and FRP functionality, we demonstrate that FRP could be wedged in the OCP's cavity, weakening the PBS and OCP interaction. Some cyanobacterial species contain small amounts of the16 kDa red carotenoid protein (RCP) that, most probably, is formed in a cyanobacterial cell by the limited proteolysis followed by a loss of the C-terminal domain of the OCP (Chábera, Durchan, Shih, Kerfeld, & Polívka, 2011; Kerfeld, 2004). Like the OCP, the RCP is also capable of quenching the PBS fluorescence (Leverenz et al., 2014). The same OCP's attachment site on the PBS surface also could participate in RCP docking, as was revealed by our simple molecular modeling.

2. Methods

The 3D structure of OCP–APC trimer complex as well as of OCP–FRP complex were explored using the Hex Protein Docking online service with standard settings (Macindoe, Mavridis, Venkatraman, Devignes, & Ritchie, 2010). Proteins were considered as rigid bodies interacting through electrostatic and Van der Waals forces. The initial coordinates of protein atoms to built up 3D models were obtained from Protein Data Bank: 1M98 (UniProt sequence P83689) for OCP from *Arthrospira maxima* (Kerfeld et al., 2003), 4JDX (P74103) for FRP from *Synechocystis* (Sutter et al., 2013), and code 1ALL

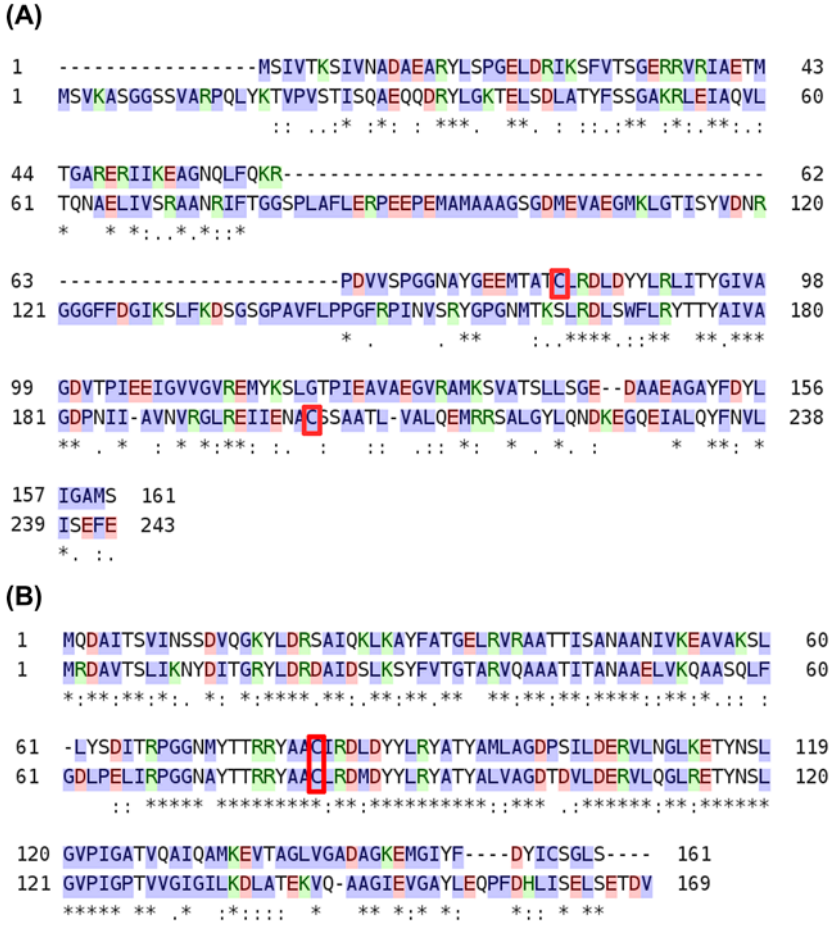

Figure 3. Pair alignment of primary sequences of αAPC (P72504) with PBL_{CM} (K1WBP7) (A) and βAPC (P72505) with β^{18} (D4ZTI6) (B) from PBS of *A. platensis*. Positively charged residues are highlighted with green color, negative – with red and hydrophobic – with violet. Residues Cys81 of αAPC, Cys201 of PBL_{CM}, Cys81 of βAPC, and Cys82 of β^{18}, which bind a chromophore molecule are marked with a red frame.

(P72504 for αAPC and P72505 for βAPC) for the $(\alpha\beta)_3$ APC trimer from *Arthrospira platensis* (Brejc et al., 1995). The highest scored OCP–APC and OCP–FRP complex structures represent the most likely mutual orientation of proteins in the assemblies. Homology-based 3D molecular model of the PB polypeptide domain of L_{CM} (K1WBP7, 19–243 a.a.), which is homologous to αAPC (29.8 % of identical positions outside the PB loop region, Figure 3(A)) was created (Figure 4(A)) using the MODELLER software (Baker, Sept, Joseph, Holst, & McCammon, 2001). The 3D structure of the β^{18}-polypeptide (D4ZTI6), which is highly homologous to βAPC polypeptide (identity 55.9 %, Figure 3(B)) was also created through homology modeling (Figure 4(B)). Coordinates of obtained earlier OCP–APC trimer complex (Figure 2 and Stadnichuk et al., 2013) were used as a reference to achieve smooth optimization of PBL_{CM} geometry with a standard automodel class for the whole structure model (19–243 a.a. region of ApcE) and loop-model class for a loop region (77–117 a.a. in full ApcE

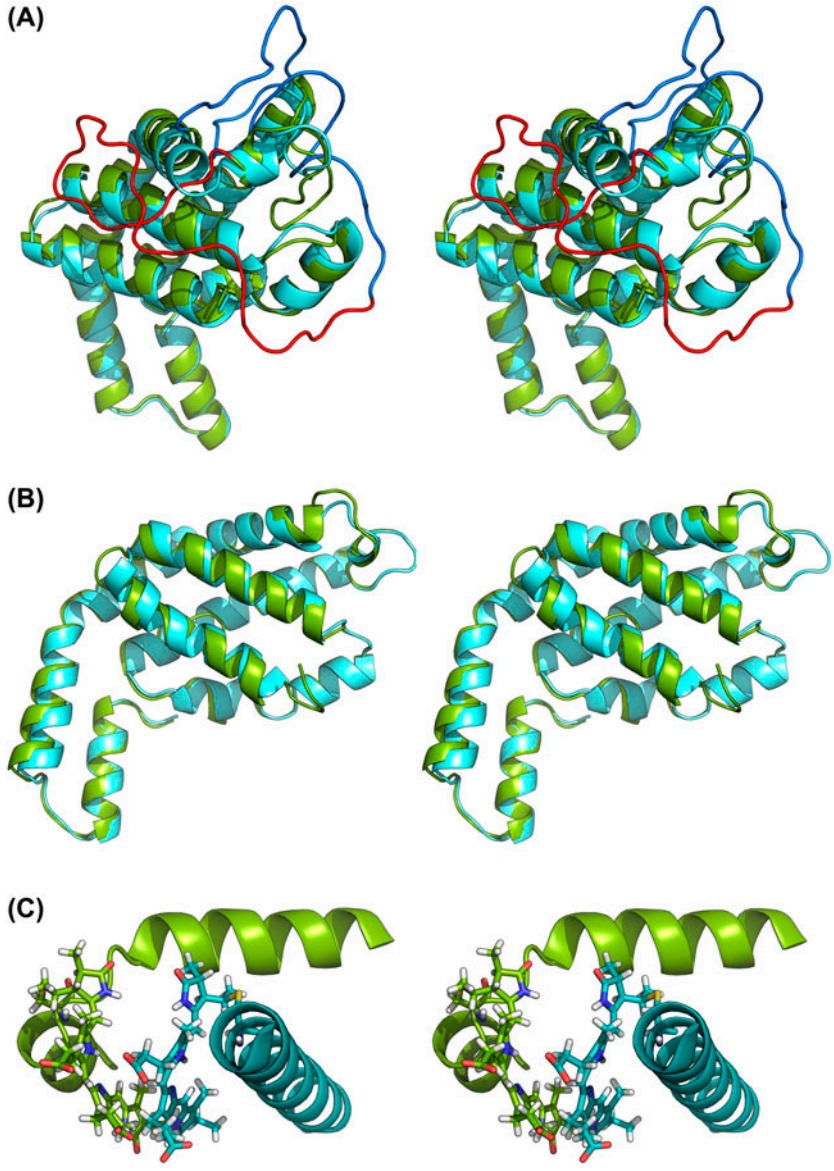

Figure 4. Stereo views of homology-based 3D models. (A) A 3D model demonstrating structural similarity between the PB domain of LCM and αAPC (cyan). The highly homologous to αAPC part of PBL_{CM} is shown in green. The flexible part of the PB loop is shown in red color, and the rigid one – in blue. The phycobilin chromophores here and in Fig. 4B are not shown for clarity. (B) A high similarity model of the β^{18} polypeptide (green) and βAPC (cyan). (C) PBL_{CM} (green) and αAPC (cyan) phycobilin cromophore relative positions in their protein binding pockets. PBL_{CM} chromophore is bound to the opposite side of the pocket and thus displaced toward the protein surface.

gene sequence, K1WBP7, or 59–119 a.a. in corresponding αAPC sequence, P72504, or PB domain) refinement. The conformation of a long (60 a.a.) PB loop could not be accurately revealed through homology modeling because of the absence of similarity of this fragment to any known protein with resolved structure. Nevertheless, our assumption that PB loop participates in the PBS–OCP interaction allowed us to choose one of the conformations, where the PB loop is fully pushed into the central cavity of OCP. The phycobilin chromophore of the PBL_{CM} was placed in the corresponding apoprotein pocket to achieve chromophore position analogous to the αAPC, but not exactly the same (Figure 4(C)). The GROMACS software package was used to determine the area of the interaction interface by the SASA algorithm with a sample particle radius equal to 1.4 Å and for geometry optimization (Pronk et al., 2013). Proposed solid geometry of the 16 kDa RCP based on the known proteolysis sites (Kerfeld, 2004; Leverenz et al., 2014) was used to build up the RCP–PBS core model. The final geometrical models of all complexes were optimized with GROMACS software (Pronk et al., 2013) with the no steric clash. All structural visualizations were performed using the PyMOL Molecular Graphics System.

3. Results

3.1. Molecular model of OCP–PBS interaction

The salient lateral surface of the APC trimer discs could easily be accessed by other proteins. The visual analysis reveals that the shape of characteristic tip on the lateral surface of the APC trimer corresponds well to the shape of the OCP central cavity located between N- and C-terminal domains of this protein (Figure 5). So, we have tested if the interaction between the APC tip and OCP cavity is possible through simple rigid-body docking procedure (HEX, Macindoe et al., 2010). The top 10 results of HEX protein docking calculations were approximately the same: the tip of αAPC was located inside the OCP central cavity. All obtained conformations have the effective energy values much below zero (E_{tot} = –4000 to 5000 kJ/mole), and differ only in the OCP orientation angle. The top scored structure with a long axis of OCP molecule orientation within the APC trimer plane has a value of E_{tot} = –5103 kJ/mole, and the total area of intermolecular interface of 2600 Å^2. This value is enough low and calculated area is enough sufficient to decide that obtained conformation is reasonable. The complementarity of OCP and APC trimer surfaces is also confirmed by quantification of hydrogen bonds possibly formed between interacting proteins. According to the obtained model, the 19 hydrogen bonds could be formed by OCP molecule: 16 with αAPC polypeptide and 3 with βAPC (Table 1). Besides, a hydrophobic contact can be realized inside the OCP cavity: hydrophobic

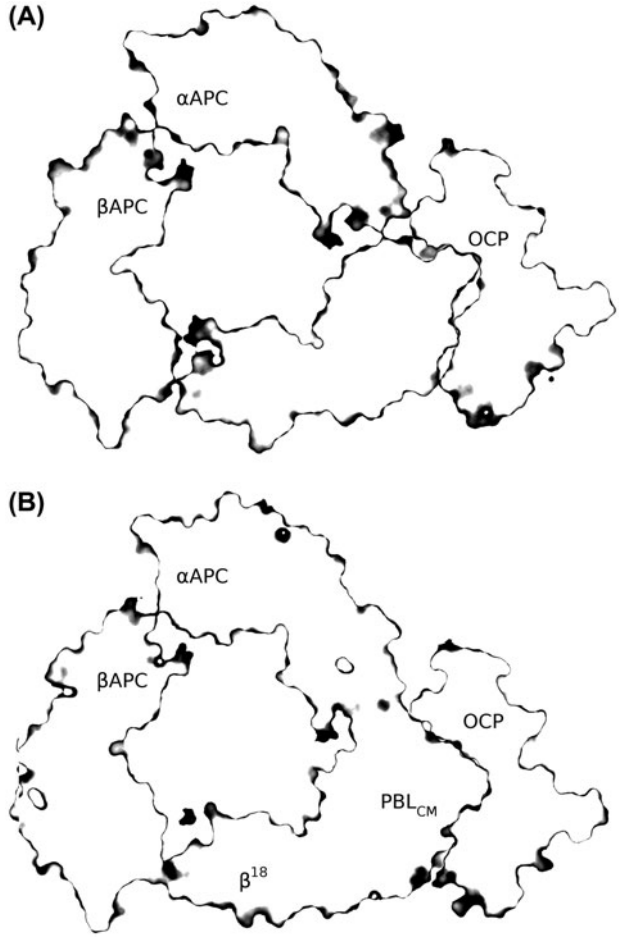

Figure 5. Slices of the $(\alpha\beta)_3$–OCP (A) and $(\alpha\beta)_2(PBL_{CM}\beta^{18})$–OCP (B) complexes were made in PyMOL environment quite parallel to the face plane of the trimers. Only the protein surfaces are shown. The slits distinctly seen between APC and OCP surfaces (A) disappear in $(\alpha\beta)_2(PBL_{CM}\beta^{18})$–OCP complex (B).

residues on the apex of the αAPC tip (P68, G69, and Y73) maintain a close contact with the OCP residues P103 and V159. All these data allow us to propose that interaction between the central cavity of OCP and the tip on the surface of αAPC in $(\alpha\beta)_3$-trimer is possible and could be realized. Moreover, the distance between centers of mass of carotenoid cofactor of OCP and phycobilin cofactor of αAPC appears to be quite short (~ 21 Å, Stadnichuk et al., 2013), which is of great importance for the efficiency of energy transfer. Cofactors are drawn together closer than in the other known recent OCP–PBS interaction model (Zhang et al., 2014). Besides, in constructed model the native spatial structures of both the OCP and PBS core stay intact, which is not true for the case (Zhang et al., 2014).

Because of the absence of any structural data for the $(\alpha\beta)_2(PBL_{CM}\beta^{18})$ trimer of the PBS core, we have utilized the possibility of its computer modeling. The amino

Table 1. Hydrogen bonds between the APC trimer and OCP molecule in complex, according to HEX protein docking server (Macindoe et al., 2010).

PBS residue		OCP residue	PBS residue		OCP residue
αAPC	E48 side chain	R9 side chain	αAPC	Cofactor molecule	K29 side chain
	R63 side chain	S166 side chain		Cofactor molecule	R89 side chain
	D64 pept Hsz	K166 side chain		E76 side chain	A26 pep H
	S67 side chain	Y171 side chain		E48 side chain	R9 side chain
	P68 pep O	T165 side chain		E48 side chain	K231 side chain
	G69 pept O	R89 side chain		K52 side chain	I5 pep O
	G70 pept H	T165 side chain	βAPC	K53 side chain	R89 pep O
	G70 pept O	R89 side chain		E54 side chain	N88 side chain
	N71 side chain	D164 side chain		K58 side chain	E34 side chain
	N71 side chain	D164 pep H			

acid sequence alignment shows that the β^{18} polypeptide is highly homologous (identity 55.9 %) to the APC β-subunit (Figure 3(B)) while the primary structure of the PBL_{CM} domain is similar to that of αAPC (Figure 3(A) and Adir, 2005; Watanabe & Ikeuchi, 2013). The 3D structure of the β^{18} polypeptide built through the homology modeling using MODELLER software (Baker et al., 2001) was found to be very similar to the crystal structure of the βAPC (Figure 4(B)). Hence, one of the β polypeptides was virtually extracted from the APC-trimer disk (presented in Figure 2) and substituted with the β^{18} polypeptide. As an intermediary energy carrier to PBL_{CM} from the bulk APC (Adir, 2005; Watanabe & Ikeuchi, 2013), the β^{18}-subunit in the obtained model is the nearest neighbor of PBL_{CM} with closest apposition of their chromophores (Figure 6).

The PB domain of L_{CM} demonstrates high (29.8 % of identical a.a.) primary structure similarity to the αAPC (Figure 3(A), and McGregor et al., 2008; Gao et al., 2012), except for the 59–119 a.a. region, known as PB loop which is of presently unknown function. The deletion of the PB loop does not influence the PBS assemblage, the attachment of PBS to the thylakoid membrane, and energy transfer from PBS to chlorophyll (Ajlani & Vernotte, 1998). Also, it does not attribute to auto-chromophorylation of L_{CM} (Gao et al., 2012). So, we have proposed that the PB loop could participate in OCP attachment. This assumption is fortified by spatial localization of the PB loop. Its peptide ends, according to the primary structure of PBL_{CM} and to the primary and tertiary structure of APC (Figure 4(A) and Capuano, Braux, Tandeau de Marsac, & Houmard, 1991), are situated exactly on the top of the αAPC tip. This allowed us to propose that the PB loop could fill the free residual volume inside the OCP central cavity in $(\alpha\beta)_3$–OCP complex (Figure 5(A)). The realized folding of the PB loop

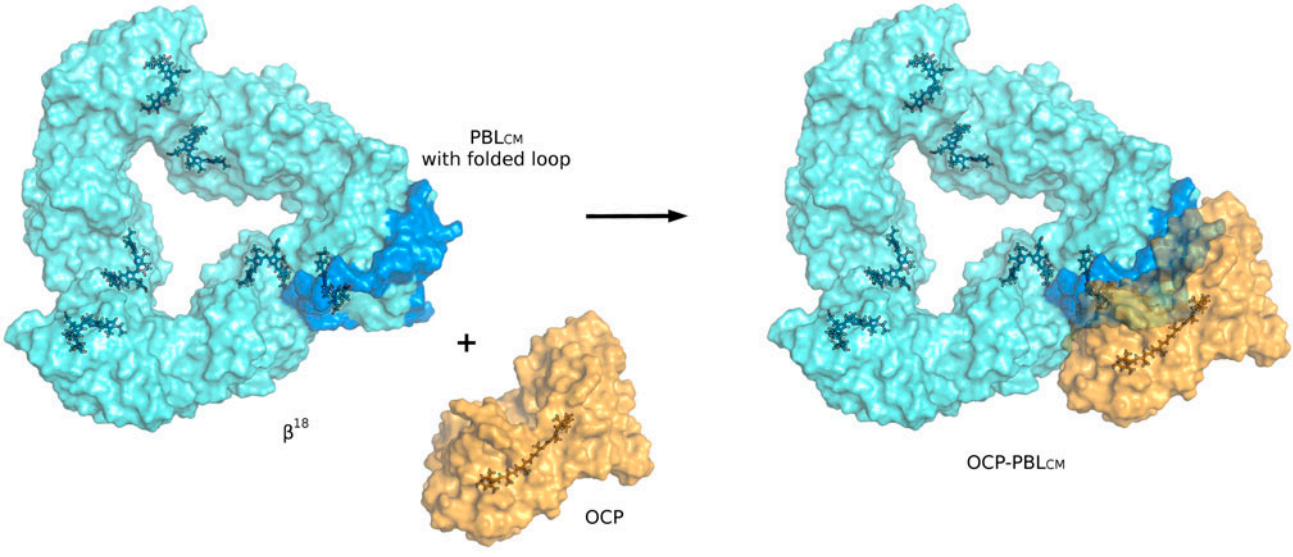

Figure 6. Constructed 3D model of the OCP–PBS interaction. The OCP (orange) is attached to the $(\alpha\beta)_2(PBL_{CM}\beta^{18})$-trimer (cyan) of the PBS core; the region of the folded PB loop is designated by blue color.

(through loop-refine class of MODELLER software) using the complete APC–OCP complex (Stadnichuk et al., 2013) as a template allowed us to create a conformation, where the first 35 residues (59–93 a.a.) of the PB loop are localized inside the OCP cavity. There was only one such conformation found among 50 different variants from MODELLER software. In this conformation, all the free volume within the OCP central cavity appears to be filled with PBL_{CM} and both proteins are a perfect match (Figure 5(B)). DOPE score for PB loop region of 59–93 a.a. is very good with the mean value of –0.047. The maximum DOPE value (–0.025) is located on the triple alanine fragment (78–80 a.a.). The rest of the PB loop (94–119 a.a.) is located outside the OCP central cavity (Figure 6) and has much worse mean DOPE value (–0.026), with zero values on glycine dimer (104–105 a.a.), presented in the center of outside part of the PB loop. Therefore, we conclude that using an $(\alpha\beta)_3$–OCP complex as a template, we have got a verisimilar conformation for the first 35 a.a. residues of the PB loop which fill the emptiness within the formed $(\alpha\beta)_2(PBL_{CM}\beta^{18})$–OCP complex. The PB loop geometry of the last 26 a.a. residues loop may vary in comparison with the one shown in Figure 6.

After the GROMACS (Pronk et al., 2013) geometry optimization, there are 22 hydrogen bonds revealed between $(\alpha\beta)_2(PBL_{CM}\beta^{18})$ trimer and OCP molecule (Table 2). Five of them bind OCP to the β^{18} polypeptide and another five to the non-PB loop part of PBL_{CM}. The other 12 hydrogen bonds are formed between OCP molecule and the PB loop, which additionally reflects loop localization inside the OCP cavity. It is important to note that both residues forming a salt bridge within the central cavity in the crystal structure of OCP (R155 and E246, Wilson et al., 2012) are involved in hydrogen bonds formation, but the salt bridge is also kept in our model. As a result, residues I288, L307, and V275 of the OCP molecule form hydrophobic contact with L64, A64, F66, and L67 residues of PBL_{CM}. The second small contact is formed by P232 and F244 of the OCP and F58 and L64 of PBL_{CM}.

The central cavity region in the interface of the N- and C-terminal domains contains plenty of water molecules (Wilson et al., 2010). The PB loop adjoins OCP, supplants the water inside the OCP cavity, and therefore enlarges the calculated total contact area from 2600 $Å^2$ in the OCP–APC complex (Figure 2) to 3900 $Å^2$ in the constructed OCP–$(\alpha\beta)_2(PBL_{CM}\beta^{18})$ complex (Figure 6). In conjunction with high spatial complementarity, we could conclude that OCP interaction with PBL_{CM} should be more favorable than with the αAPC and we assume that it could be realized in biochemically established (Gwizdala et al., 2011; Stadnichuk et al., 2011) OCP–PBS interaction system.

In αAPC, the Cys81 covalently binds the chromophore molecule, but in PBL_{CM} a homologous residue is substituted for serine (Ser163, Figure 3(A)) that cannot attach the phycobilin. In PBL_{CM}, phycobilin is covalently bound to the Cys201 residue (Figure 3(A)) which is located opposite to the αAPC side of the chromophore binding pocket (Figure 4(C)). As a result (Gao et al., 2012; McGregor et al., 2008) and also because of the PB loop folding, the chromophore molecule of PBL_{CM} is pulled closer to the outside surface of the protein. The resulting computed chromophore coordinates were used to determine the distance between the carotenoid in OCP and the nearest phycobilin chromophore belonging to PBL_{CM}. The distance between centers of mass of the two pigments was determined to be 24.7 Å. Since PBL_{CM} accumulates energy from most of the dozens of short-wavelength chromophores of the PBS (Adir, 2005; Watanabe & Ikeuchi, 2013), the only revealed single carotenoid-phycobilin quenching pair of OCP–PBL_{CM} could suffice as a quenching center (Stadnichuk et al., 2012, 2013).

Table 2. Hydrogen bonds between $(\alpha\beta)_2(PBL_{CM}\beta^{18}$ and OCP molecule in complex, according to HEX protein docking server (Macindoe et al., 2010).

PBS residue		OCP residue	PBS residue		OCP residue
PBL_{CM}	P145 pep O	T165 side chain	Loop	E92 pep O	K231 side chain
	P145 pep O	D64 pep H		G99 pep O	N 156 side chain
	E198 side chain	K167 side chain		E107 side chain	D91 pep H
	C201 pep O	K167 side chain		T113 side chiain	K167 side chain
	Cofactor	R89 side chain		R120 side chain	S166 side chain
loop	S80 pep H	R241 pep O		R120 side chain	S166 pep O
	L82 pep H	E246 side chain	β_{18}	K53 side chain	N88 pep O
	A83 pep H	E246 side chain		Q54 side chain	N88 side chain
	F84 pep O	R155 side chain		S57 pep O	L31 pep H
	R87 side chain	D19 side chain		Q58 side chain	E34 side chain
	R87 side chain	D306 side chain		G61 pep H	Q30 side chain

3.2. Molecular model of the OCP–FRP interaction

The 3D models of the complex formed by OCP with the $(\alpha\beta)_3$-trimer of APC (Figure 2 and Stadnichuk et al., 2013) and the $(\alpha\beta)_2(PBL_{CM}\beta^{18})$-trimer (Figure 6) revealed the decisive importance of the central cavity of the OCP in the OCP–PBS interaction. Remarkably, the cavity surface ideally faces a very characteristic tip jutting from the lateral bulge of both varieties of PBS core-trimers (Figures 2 and 6). Besides, the PB loop in the primary structure of L_{CM} is located exactly within this tip region. The role of the intradomain cavity of the OCP was verified in a model of another known interaction of OCP with the FRP (Figure 7) during restoration of normal antenna capacity of the PBS (Boulay et al., 2010).

The FRP consists only of α-helices and short disordered loops that connect structured fragments and form an extended helical stalk and a compact head domain (Sutter et al., 2013). In the resulting 3D crystal structure, the FRP was found in dimeric and tetrameric states. Efforts to generate the tetramer in a solution were not successful; the dimer form (Figure 7(A)) is predominant, and the larger form might be a dimer of dimers as a side effect of the concomitant crystallization procedures (Sutter et al., 2013). Therefore, we have concentrated on the modeling of the interaction of the OCP with the monomeric and dimeric forms of the FRP and have performed docking of full-length FRP monomer and FRP dimer with the OCP molecule. It should be noted that on the FRP surface there is a bulge resembling the αAPC tip (Figure 7). We have proposed that this bulge may also be involved in the interaction with OCP molecule. This proposition was confirmed through docking experiments. In most of the first 100 resulting structures, the bulge on the FRP surface had come inside the OCP central cavity. The details of these complexes are variable. First of all, the FRP molecule may be rotated conversely against the OCP molecule. But the first five structures with E_{tot} value in the range of –4000 to –4500 kJ/mole had the same mutual orientation of OCP and FRP molecules (Figure 7(B)). The most convincing solution based on the score (E_{tot} = –4580 kJ/mole) and surface complementarity places the FRP monomer molecule in the same central cavity of the OCP as the $(\alpha\beta)_2(PBL_{CM}\beta^{18})$-trimer does (Figure 7(B)). The calculated summary contact area between the OCP and the monomeric FRP form was about 2550 Å^2, which makes it approximately equal to the surface area of the interface in OCP–PBS complex. There are 11 hydrogen bonds between FRP and OCP molecules, that is less than in modeled OCP–APC and OCP–$(\alpha\beta)_2(PBL_{CM}\beta^{18})$ complexes, but is quite sufficient for binding (Table 3). The striking feature of this model is the complete similarity of the interaction interface of OCP and the ~100 kDa APC trimer with the interface of the OCP and FRP (only 13 kDa). In this interaction, the head domain of the FRP molecule plays the role of an APC tip. Tested by coimmunoprecipitation, the attachment of the C- and N-terminal domains of the OCP to the FRP had shown that only the C-terminal domain precipitates with the FRP (Kirilovsky & Kerfeld, 2013). This result correlates with our model (Figure 7(B)) where the C-terminal domain of the OCP interacts both with head and stalk domains of the FRP, while the N-terminal domain is in contact only with a part of its compact head domain. The very probable coincidence of interaction of FRP and of PBS with the same OCP's central cavity allows us to propose the competitive mechanism of FRP function, which interacts with the OCP and prevents its attachment to the PBS surface.

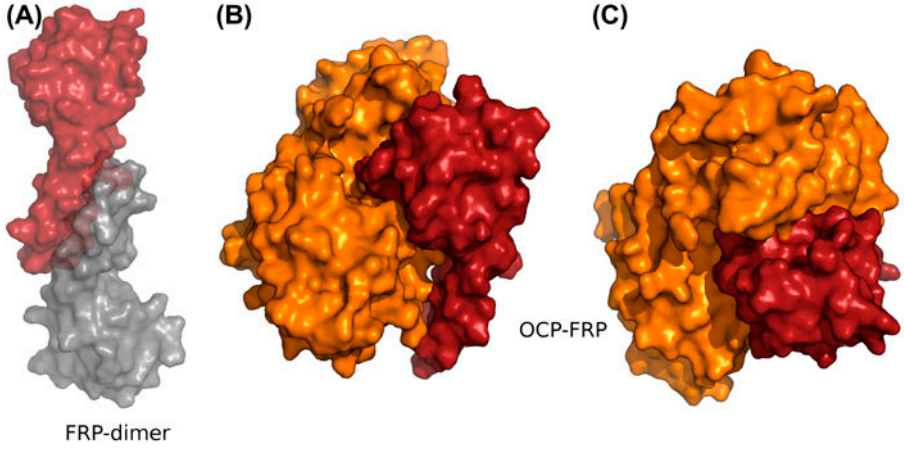

Figure 7. Constructed 3D model of OCP–FRP interaction. (A) 3D structure of FRP dimer according to 4JDX code of PDB; two identical monomers of FRP are shown in red and gray for clarity. (B, C) Two projections of FRP (red) and OCP (orange) complex model. The head domain of monomeric FRP interacts with the central cavity of OCP.

Table 3. Hydrogen bonds between the FRP and OCP molecule in complex, according to HEX protein docking server (Macindoe et al., 2010).

FRP residue	OCP residue	FRP residue	OCP residue
E53 side chain	R164 side chain	Q112 side chain	R89 pep O
E87 side chain	R164 side chain	G110 pep O	F163 pep H
G90 pep O	R239 side chain	K133 side chain	S29 pep O
K108 side chain	N156 side chain	L134 carb O	N156 side chain
K108 pep O	K106 side chain	L134 carb O	Q228 side chain
E109 pep O	K106 side chain		

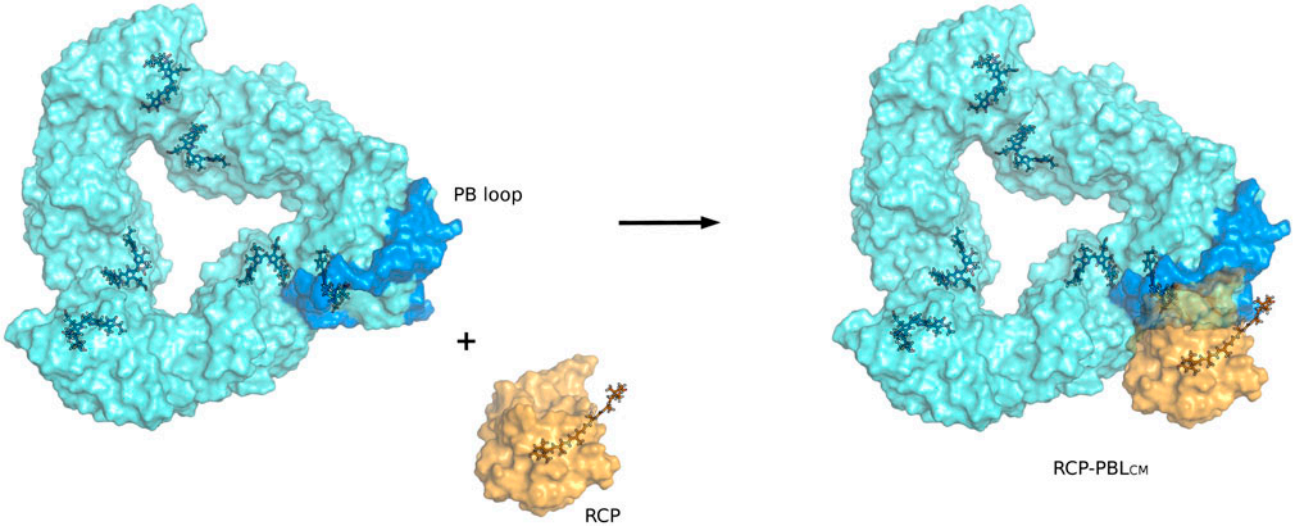

Figure 8. Proposed 3D model of RCP (orange) and $(\alpha\beta)_2(PBL_{CM}\beta^{18})$-trimer (cyan) within the PBS core. The folded loop of PBL_{CM} (blue) has larger contact area with the RCP than β^{18} polypeptide does.

3.3. Molecular model of the RCP–PBS interaction

It is proposed that while the OCP triggers the NPQ, the primarily role of the RCP obtained proteolytically from the OCP is scavenging singlet oxygen possibly produced in high light by PBS (Chábera et al., 2011). In this case, our modeling procedure was based on the hypothetical model of the RCP originated from OCP by the loss of C-terminal domain and retaining N-terminal domain and carotenoid chromophore (Kerfeld, 2004; Leverenz et al., 2014). In the model (Figure 8 and Kerfeld, 2004), the carotenoid molecule retained in RCP is partly accessible to surrounding solution. This model is much more speculative than previously described, but it could be considered as a zero-order approximation. Our analysis demonstrates that in the obtained model of OCP–$(\alpha\beta)_2(PBL_{CM}\beta^{18})$ interaction (Figure 6), the OCP molecule can be easily substituted by the RCP. As seen from Figure 8, the folded PB loop plays the main role in the estimated spectroscopical (Leverenz et al., 2014) interaction of the PBS and RCP while the PBS loop has a larger contact area with the RCP than β^{18}-subunit has.

4. Discussion

Due to the bulky PBS superstructure, it is not clear a priori where and how the OCP is attached to the PBS core. Lack of structural data of OCP^r also prevented its final assignment in the PBS. The exact binding site of the OCP and PBS will be completely elucidated only after crystal structure data for the PBS core become known. It was hypothesized that OCP can bind to any bulk APC_{660} trimers, which implies several nonspecific binding sites per PBS (Kirilovsky & Kerfeld, 2013). This assumption is difficult to combine with current lack of evidence of the interaction between OCP and isolated APC trimers in solution (Stadnichuk et al., 2012). An earlier suggestion that OCP could interact with the PBS only via its C-terminal domain (Wilson et al., 2008) was based on the structural similarity of this domain and the small $L_{7.8}$ core linker protein of the PBS. The model is in contradiction with the constant disposition of $L_{7.8}$ in the external trimers of the APC-built cylinders in the PBS core (Adir, 2005). This suggestion was reconsidered in favor of the N-terminal domain on assumption of

involving of positively charged Arg155 residue in the N-terminal OCP domain into an interaction with PBS (Wilson et al., 2010). Recently, the participation of L_{CM} in anchoring the OCP was confirmed by chemical cross linking of L_{CM} surface lysine residue with OCP during OCP^r and PBS interaction. On the basis of protein cross-linking, the OCP was possibly buried between two APC trimers of the PBS, one of which contains PBL_{CM} (Zhang et al., 2014). Nevertheless, under this assumption, the closest distance between carotenoid and the nearest phycobilin molecule is greater (25.8 Å, Zhang et al., 2014) than in our model (24.7 Å). As the distance length strongly dictates the efficiency of energy transfer, this hypothesis is not free from shortcomings either.

Our model has some serial advantages. First of all, the discerning of PBL_{CM} as the attachment site for OCP from the bulk APC is easily explained by the interaction of OCP with the folded PB loop present in L_{CM}. Also, in our model, the attachment of OCP to the PBS surface could affect by hydrogen bonds formation the salt bridge between Arg155 and Glu244, which are in the interface between the N- and C-terminal domains in the central OCP cavity (Kerfeld, 2004). In our static crystal structures-based model, the salt bridge remains intact, but in real flexible system this bond could be broken. It was demonstrated earlier, by site-directed mutagenesis, that the salt bridge between the Arg155 and Glu244 residues in OCP^r is really nonexistent (Wilson et al., 2010). Besides (see above), the determined distance between the OCP's carotenoid and nearest phycobilin of PBL_{CM} is very reasonable because it does not exceed the distances between phycobilin chromophores known for APC and for other phycobiliproteins of the PBS (Adir, 2005). In conclusion, the important feature of our model is its universality: it is the obligatory participation of intra-domain OCP's cavity and one of the similar characteristic tips on the αAPC, $PBL_{CM,}$ or FRP surfaces in attachment site formation in all proposed complexes.

Disclosure statement

No potential conflict of interest was reported by the authors.

Funding

This work was supported by the Russian Science Foundation (Project 14-14-00589).

References

Adir, N. (2005). Elucidation of the molecular structures of components of the phycobilisome: Reconstructing a giant. *Photosynthesis Research, 85*, 15–32.

Ajlani, G., & Vernotte, C. (1998). Deletion of the PB-loop in the L_{CM} subunit does not affect phycobilisome assembly or energy transfer functions in the cyanobacterium *Synechocystis* sp. PCC6714. *European Journal of Biochemistry, 257*, 154–159.

Baker, N., Sept, D., Joseph, S., Holst, M., & McCammon, A. (2001). Electrostatics of nanosystems: Application to microtubules and the ribosome. *Proceedings of the National Academy of Sciences USA, 98*, 10037–10041.

Boulay, C., Wilson, A., D'Haene, S., & Kirilovsky, D. (2010). Identification of a protein required for recovery of full antenna capacity in OCP-related photoprotective mechanism in cyanobacteria. *Proceedings of the National Academy of Sciences USA, 107*, 11620–11625.

Brejc, K., Ficner, R., Huber, R., & Steinbacher, S. (1995). Isolation, crystallization, crystal structure analysis and refinement of allophycocyanin from the cyanobacterium Spirulina platensis at 2.3 Å resolution. *Journal of Molecular Biology, 249*, 424–440.

Capuano, V., Braux, A.-S., Tandeau de Marsac, N., & Houmard, J. (1991). The "anchor polypeptide" of cyanobacterial phycobilisomes. Molecular characterization of the *Synechococcus* sp. PCC 6301 *apcE* gene. *Journal of Biological Chemistry, 266*, 7239–7247.

Chábera, P., Durchan, M., Shih, P., Kerfeld, C., & Polívka, T. (2011). Excited-state properties of the 16kDa red carotenoid protein from Arthrospira maxima. *Biochimica et Biophysica Acta (BBA) – Bioenergetics, 1807*, 30–35.

Gao, X., Wei, T., Zhang, N., Xie, B., Su, H., Zhang, X. Y., & Zhang, Y. Z. (2012). Molecular insights into the terminal energy acceptor in cyanobacterial phycobilisome. *Molecular Microbiology, 85*, 907–915.

Gwizdala, M., Wilson, A., & Kirilovsky, D. (2011). *In vitro* reconstitution system of the cyanobacterial photoprotective mechanism mediated by the orange carotenoid protein in *Synechocystis* PCC 6803. *Plant Cell, 23*, 2631–2643.

Gwizdala, M., Wilson, A., Omari-Nasser, A., & Kirilovsky, D. (2013). Characterization of the synechocystis PCC 6803 fluorescence recovery protein involved in photoprotection. *Biochimica et Biophysica Acta (BBA) – Bioenergetics, 1827*, 348–354.

Holt, T., & Krogmann, D. (1981). A carotenoid protein from cyanobacteria. *Biochimica et Biophysica Acta (BBA) – Bioenergetics, 637*, 408–414.

Jallet, D., Gwizdala, M., & Kirilovsky, D. (2012). ApcD, ApcF and ApcE are not required for the Orange Carotenoid Protein related phycobilisome fluorescence quenching in the cyanobacterium Synechocystis PCC 6803. *Biochimica et Biophysica Acta (BBA) – Bioenergetics, 1817*, 1418–1427.

Kerfeld, C. (2004). Structure and function of the water-soluble carotenoid-binding proteins of cyanobacteria. *Photosynthesis Research, 81*, 215–225.

Kerfeld, C., Sawaya, M. R., Vishnu, B., Cascio, D., Ho, K. K., Trevithick-Sutton, C. C., … Yeates, T. O. (2003). The crystal structure of a cyanobacterial water-soluble carotenoid binding protein. *Structure, 11*, 55–65.

Kirilovsky, D., & Kerfeld, C. (2013). The orange carotenoid protein: A blue–green light photoactive protein. *Photochemical & Photobiological Sciences, 12*, 1135–1143.

Leverenz, R., Jallet, D., Li, M., Mathies, R., Kirilovsky, D., & Kerfeld, C. (2014). Structural and functional modularity of the orange carotenoid protein: Distinct roles for the N- and C-terminal domains in cyanobacterial photoprotection. *The Plant Cell, 26*, 426–437.

Macindoe, G., Mavridis, L., Venkatraman, V., Devignes, M., & Ritchie, D. (2010). HexServer: An FFT-based protein docking server powered by graphics processors. *Nucleic Acids Research, 38*, W445–W449.

McGregor, A., Klartag, M., David, L., & Adir, N. (2008). Allophycocyanin trimer stability and functionality are primarily due to polar enhanced hydrophobicity of the phycocyanobilin binding pocket. *Journal of Molecular Biology, 384*, 406–421.

Pronk, S., Páll, S., Schulz, R., Larsson, P., Bjelkmar, P., Apostolov, R., & Lindahl L. (2013). GROMACS 4.5: A high-throughput and highly parallel open source molecular simulation toolkit. *Bioinformatics, 29*, 845–854.

Rakhimberdieva, M., Stadnichuk, I., Elanskaya, I., & Karapetyan, N. (2004). Carotenoid-induced quenching of the phycobilisome fluorescence in photosystem II-deficient mutant of *Synechocystis* sp. *FEBS Letters, 574*, 85–88.

Scott, M., McCollum, C., Vasil'ev, S., Crozier C, Espie GS, Krol M, … Bruce D. (2006). Mechanism of the down regulation of photosynthesis by blue light in the cyanobacterium *Synechocystis* sp. PCC 6803. *Biochemistry, 45*, 8952–8958.

Stadnichuk, I., Lukashev, E., & Elanskaya, I. (2009). Fluorescence changes accompanying short-term light adaptations in photosystem I and photosystem II of the cyanobacterium Synechocystis sp. PCC 6803 and phycobiliprotein-impaired mutants: State 1/State 2 transitions and carotenoid-induced quenching of phycobilisomes. *Photosynthesis Research, 99*, 227–241.

Stadnichuk, I., Yanyushin, M., Bernát, G., Zlenko, D., Krasilnikov, P., Lukashev, E., … Paschenko V. (2013). Fluorescence quenching of the phycobilisome terminal emitter L_{CM} from the cyanobacterium *Synechocystis* sp. PCC 6803 detected *in vivo* and *in vitro*. *Journal of Photochemistry and Photobiology B: Biology, 125*, 137–145.

Stadnichuk, I., Yanyushin, M., Maksimov, E., Lukashev, E., Zharmukhamedov, S., Elanskaya, I., & Paschenko, V. (2012). Site of non–photochemical quenching of the phycobilisome by orange carotenoid protein in the cyanobacterium *Synechocystis* sp. PCC 6803. *Biochimica et Biophysica Acta (BBA) – Bioenergetics, 1817*, 1436–1445.

Stadnichuk, I., Yanyushin, M., Zhgarmukhamedov, S., Maksimov, E., Muronets, E., & Paschenko, V. (2011). Quenching of phycobilisome fluorescence by orange carotenoid–protein. *Doklady Biochemistry and Biophysics, 439*, 167–170.

Sutter, M., Wilson, A., Leverenz, R., Lopez-Igual, R., Thurotte, A., Salmeen, A., … Kerfeld C. (2013). Crystal structure of the FRP and identification of the active site for modulation of OCP–mediated photoprotection in cyanobacteria. *Proceedings of the National Academy of Sciences USA, 110*, 10022–10027.

Watanabe, W., & Ikeuchi, M. (2013). Phycobilisome: Architecture of a light-harvesting supercomplex. *Photosynthesis Research, 116*, 265–276.

Wilson, A., Ajlani, G., Verbavatz, J., Vass, I., Kerfeld, C., & Kirilovsky, D. (2006). A soluble carotenoid protein involved in phycobilisome-related energy dissipation in cyanobacteria. *The Plant Cell online, 18*, 992–1007.

Wilson, A., Gwizdala, M., Mezzettti, A., Alexandre, M., Kerfeld, C., & Kirilovsky, D. (2012). The essential role of the N-terminal domain of the orange carotenoid protein in cyanobacterial photoprotection: Importance of a positive charge for phycobilisome binding. *The Plant Cell, 24*, 1972–1983.

Wilson, A., Kinney, J., Zwart, P., Punginelli, C., D'Haene, S., Perreau, F., … Kerfeld C. (2010). Structural determinants underlying photoprotection in the photoactive orange carotenoid protein of cyanobacteria. *Journal of Biological Chemistry, 285*, 18364–18375.

Wilson, A., Punginelli, C., Gall, A., Bonetti, C., Alexandre, M., Routaboul, J., … Kirilovsky D. (2008). A photoactive carotenoid protein acting as light intensity sensor. *Proceedings of the National Academy of Sciences USA, 33*, 12075–12080.

Zhang, H., Liu, H., Niedzwiedzki, D., Prado, M., Jiang, J., Gross, M., & Blankenship, R. (2014). Molecular mechanism of photoactivation and structural location of the cyanobacterial orange carotenoid protein. *Biochemistry, 53*, 13–19.